Molecular Catalysis 494 (2020) 111113

Contents lists available at ScienceDirect

Molecular Catalysis

journal homepage: www.elsevier.com/locate/mcat

Phosphorus-loaded alumina supported nickel catalysts for CO_2 hydrogenation: Ni_2P/Ni_5P_{12} drives activity

T. Rajkumar[a], András Sápi[a,b,*], Marietta Ábel[a], Gyula Halasi[a], János Kiss[a,c], Juan Fernando Gómez-Pérez[a], Henrik Bali[a], Ákos Kukovecz[a], Zoltán Kónya[a,c]

[a] University of Szeged, Interdisciplinary Excellence Centre, Department of Applied and Environmental Chemistry, H-6720, Rerrich Béla tér 1, Szeged, Hungary
[b] Institute of Environmental and Technological Sciences, University of Szeged, H-6720, Szeged, Hungary
[c] MTA-SZTE Reaction Kinetics and Surface Chemistry Research Group, University of Szeged, H-6720, Szeged, Hungary

ARTICLE INFO

Keywords:
CO_2 hydrogenation
H_2-TPR
Phosphorus-loaded
Nickel-based catalyst
XPS

ABSTRACT

A series of 5 wt% NiO-xP-Al_2O_3 with different phosphorus loading contents (x = 0, 5, 15 and 20 wt%) were prepared by a modified sol-gel method. A significant promotional effect of phosphorus on NiO-Al_2O_3 in CO_2 hydrogenation is observed. All the catalysts reach the highest conversion at 600 °C with 61.54 %, 62.89 %, 63.88 % and 66.13 % respectively for 5 wt% NiO-Al_2O_3, 5 wt% NiO-5P-Al_2O_3, 5 wt% NiO-15P-Al_2O_3 and 5 wt% NiO-20P-Al_2O_3 catalysts. Ni/NiO/Ni_2P/Ni_5P_{12}/$AlPO_4$ interfacial species were detected on the surface as active species on the used catalysts by X-ray photoelectron spectroscopy. The formation ratio of the metal-phosphide is relatively low ~3−5 %, and this atomic concentration is decreasing with the rising of the phosphate content. However, the nickel enrichment in the surface layer presumable in Ni_2P/Ni_5P_{12} form is very likely according to the P 2p spectra and the authors assume that could be responsible for the enhanced catalytic activity.

1. Introduction

In recent years, CO_2 hydrogenation is the most important process because it not only reduces global warming but also produces value-added products [1–5]. The hydrogen obtained from water electrolysis using renewable and sustainable energy sources such as solar, wind, geothermal, biomass etc. can be used to hydrogenate CO_2 [6]. A variety of chemicals such as CO, CH_4, CH_3OH etc. can be obtained through catalytic hydrogenation of CO_2 [7–9]. CO is a valuable precursor molecule that can be used as a raw material for the production of olefins, methyl alcohols and liquid hydrocarbons for the Fischer-Tropsch synthesis [10,11]. Various precious metals including Au, Pt, Pd, Rh and Ru [12–16] and non-precious metals Ni, Fe and Cu [17–19] loaded on various supports have been reported for the production of CO.

Several metal catalyst have been reported to be active in CO_2 methanation reaction including noble metal catalysts such as Pd, Ru and Pt [20–22] and non-noble metal catalysts such as Cu, Ni and Co [19,23,24] loaded on various supports such as Al_2O_3, SiO_2, TiO_2, CeO_2 and ZrO_2 [25–29]. NiO have been extensively investigated in various fields as catalysts [30,31], sensors [32–34] as well as batteries [35,36] due to their high catalytic activity, low cost and low toxicity. γ-Alumina is widely used as a catalyst [37–39], adsorbent [40] and catalyst support [41] due its thermal, chemical and mechanical stabilities. Compared with individual performances of NiO and Al_2O_3, NiO-Al_2O_3 composites are more efficient and have been used as catalysts [42–45], batteries [46,47], sensors [48,49] and adsorbents [50,51]. The non-metal phosphorus element has been proven to serve as a structure stabilizer of alumina [52–54]. Meanwhile, the incorporation of phosphorus into alumina brings about the decoration of hydroxyl groups on the surface of alumina accompanied by the formation of P−OH groups. The dehydroxylation between P−OH groups results in the formation of P═O groups, which will rehydrate into P−OH groups in the presence of water and consequently reduce the adsorption of water on the adsorption sites of the catalysts, hence enabling the improvement of the hydrothermal stability for the NiO/Al_2O_3 catalysts. Moreover, the reducibility of metal-alumina have been found to be increased after doping phosphorus [55].

In the present work, a series of 5 wt% NiO-xP-Al_2O_3 (x = 0, 5, 15, 20 wt%) catalysts have been prepared by a modified sol-gel method and investigated their performances in CO_2 hydrogenation reaction. The results show that addition of phosphorus can significantly increase the catalytic activity. Compared with phosphorus unloaded 5 wt% NiO-Al_2O_3 catalyst, phosphorus loaded 5 wt% NiO-xP-Al_2O_3 catalysts exhibit superior performance.

* Corresponding author at: University of Szeged, Interdisciplinary Excellence Centre, Department of Applied and Environmental Chemistry, H-6720, Rerrich Béla tér 1, Szeged, Hungary.
E-mail address: sapia@chem.u-szeged.hu (A. Sápi).

https://doi.org/10.1016/j.mcat.2020.111113
Received 7 May 2020; Received in revised form 30 June 2020; Accepted 4 July 2020

2. Experimental

2.1. Chemicals

Nickel (II) nitrate hexahydrate ($Ni(NO_3)_2.6H_2O$, ≥ 98.5 %) and pluronic P-123 (average M_n ~5800) were purchased from Aldrich. Ammonium dihydrogen phosphate was purchased from Reanal. Aluminium isopropoxide (≥98 %) and acetic acid (99.7 %) were purchased from Sigma-Aldrich. Ethanol absolute (99.96 %) was purchased from VWR chemicals. Isopropanol (99.99 %) was purchased from molar chemicals. All chemicals were used as received without any further purification.

2.2. Synthesis of catalyst support

P-loaded alumina was prepared via a modified sol-gel method. 1.50 g P123 (M_{av} = 5800) was dissolved in the mixed solution of 30 mL absolute ethanol, 10 mL isopropanol and 0.18 mL acetic acid at ambient temperature. Then, a required amount of ammonium dihydrogen phosphate and 0.015 mol of aluminium isopropoxide were introduced into the above solution under vigorous stirring for 4 h. The product was dried overnight at 80 °C and calcined in air at 500 °C for 4 h and then at 1000 °C for 1 h.

2.3. Synthesis of catalysts

The as-obtained P-loaded Al_2O_3 support was loaded with 5 wt% NiO by the incipient wetness impregnation method using $Ni(NO_3)_2.6H_2O$ aqueous solution as metal precursors. The product was dried overnight at 80 °C and calcined in air at 500 °C for 1 h. The final sample was marked as 5 wt% NiO-xP-Al_2O_3 (x = 0, 5, 15, 20 wt%).

2.4. Characterization of the catalysts

2.4.1. N_2 adsorption-desorption isotherm measurements

The specific surface area (BET method), the pore size distribution and the total pore volume were determined by the BJH method using a Quantachrome NOVA 2200 gas sorption analyser by N_2 gas adsorption/desorption at −196 °C. Before the measurements, the samples were pre-treated in a vacuum at 200 °C for 2 h.

2.4.2. Powder X-ray diffraction (XRD)

XRD studies of all samples were performed on a Rigaku MiniFlex II instrument with a Ni-filtered Cu-Kα source in the range of 2θ = 20 − 80°.

2.4.3. Transmission Electron Microscopy (TEM)

Imaging of the all the samples were carried out using a FEI TECNAI G2 20 X-Twin high-resolution transmission electron microscope (equipped with electron diffraction) operating at an accelerating voltage of 200 kV. The samples were drop-cast onto carbon film coated copper grids from ethanol suspension.

2.4.4. H_2-Temperature programmed reduction (H_2-TPR)

The temperature-programmed reduction (TPR) was carried out in a BELCAT-A analyser using a reactor (quartz tube with 9 mm outer diameter) that was externally heated. Before the measurements, the 50 mg of catalyst was pre-treated in oxygen at 400 °C for 30 min and in N_2 at 400 °C for 15 min. Thereafter, the sample was cooled in flowing N_2 to 50 °C. The oxidized sample was flushed with N_2 containing 10 % H_2, the reactor was heated linearly at a rate of 5 °C/min from 50 °C to 500 °C and the H_2 consumption was detected by a thermal conductivity detector (TCD).

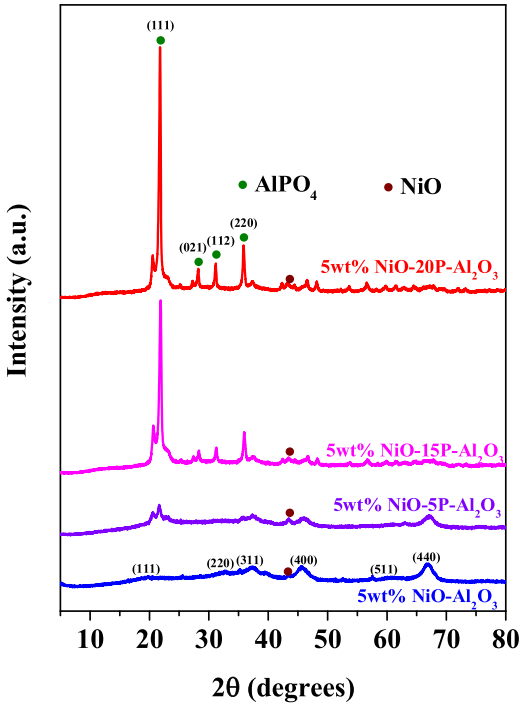

Fig. 1. XRD pattern of 5 wt% NiO-xP-Al_2O_3 (x = 0, 5, 15, 20) catalysts.

2.4.5. X-ray photoelectron spectra

The chemical states (and the atomic ratio of the elements) were investigated by X-ray photoelectron spectroscopy (XPS). The SPECS instrument was equipped with a Phoibos150 MCD-9 analyser. The Al Kα x-ray source was operated at 14 kV and 10.8 mA (150 W) and the analyser was used in FAT mode with a pass energy of 20 eV in the case of high-resolution spectra. CasaXPS software was used for data evaluation. The binding energy was set to the adventitious carbon C1 s peak is at 284.8 eV. The peaks of the P2p were fitted with single due to closely spaced spin-orbit coupling. Specs FG 15/40 flood gun was operated during the accumulation at 0.6 V and 0.3 mA to the prevent the charging of the surface of the sample.

2.4.6. Hydrogenation of carbon-dioxide in a continuous flow reactor

Before the catalytic experiments in a continuous-flow reactor the as-received catalysts were oxidized in the O_2 atmosphere at 300 °C for 30 min to remove the surface contaminants and thereafter were reduced in H_2 at 300 °C for 60 min. Catalytic reactions were carried out at atmospheric pressure in a fixed-bed continuous-flow reactor (200 mm long with 8 mm i.d.), which was heated externally. The dead volume of the reactor was filled with quartz beads. The operating temperature was controlled by a thermocouple placed inside the oven close to the reactor wall, to assure precise temperature measurement. For catalytic studies, small fragments (about 1 mm) of slightly compressed pellets were used. Typically, the reactor filling contained 150 mg of catalyst. In the reacting gas mixture, the CO_2: H_2 molar ratio was 1:4, if not denoted otherwise. The CO_2: H_2 mixture was fed with the help of mass flow controllers (Aalborg), the total flow rate was 50 mL/min. The reacting gas mixture flow entered and left the reactor through an externally heated tube in order to avoid condensation. The analysis of the products and reactants was performed with an Agilent 6890 N gas chromatograph using HP-PLOTQ column. The gases were detected

Table 1
Textural parameters of the catalysts.

Samples	BET surface area (m^2/g)	Pore volume (cm^3/g)	Average pore size (nm)
5 wt% NiO-Al_2O_3	100.52	0.26	4.19
5 wt% NiO-5P-Al_2O_3	53.91	0.10	1.67
5 wt% NiO-15P-Al_2O_3	39.13	0.09	1.81
5 wt% NiO-20P-Al_2O_3	22.67	0.06	4.92

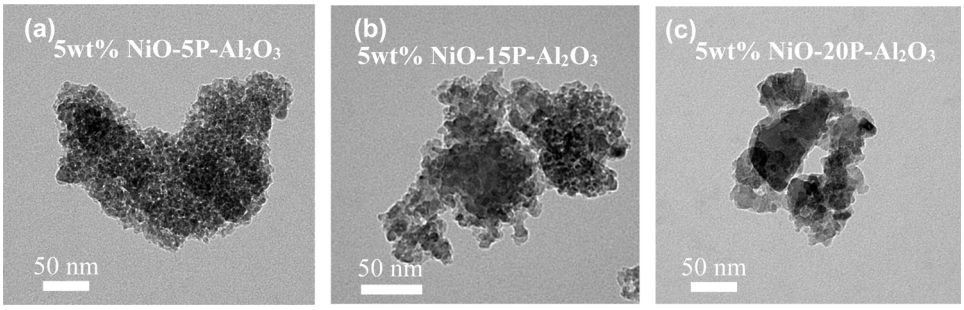

Fig. 2. TEM images of (a) 5 wt% NiO-5P-Al_2O_3 (b) 5 wt% NiO-15P-Al_2O_3 (c) 5 wt% NiO-20P-Al_2O_3.

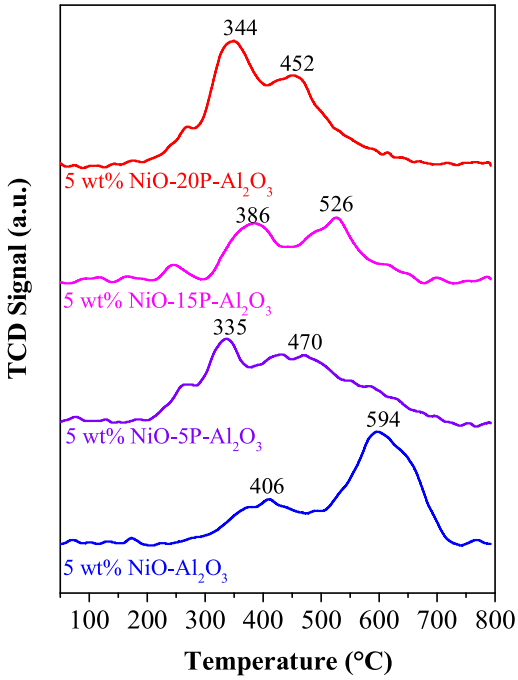

Fig. 3. H_2-TPR profile of 5 wt% NiO-xP-Al_2O_3 (x = 0, 5, 15, 20) catalysts.

Table 2
H_2 temperature-programmed reduction data for the catalysts.

Catalysts	H_2-TPR	
	Peak positions (°C)	Total H_2 consumption (mmol g^{-1})
5 wt% NiO-Al_2O_3	406, 594	0.827
5 wt% NiO-5P-Al_2O_3	335, 470	0.838
5 wt% NiO-15P-Al_2O_3	386, 526	0.764
5 wt% NiO-20P-Al_2O_3	344, 452	0.952

simultaneously by thermal conductivity (TC) and flame ionization (FI) detectors. The CO_2 was transformed by a methanizer to methane and it was also analyzed by FID. CO_2 conversion was calculated on a carbon atom basis, i.e.

$$CO_2\ \text{conversion}(\%) = \frac{CO_{2\,in} - CO_{2\,out}}{CO_{2\,in}} \times 100\%$$

CH_4 selectivity and CO selectivity were calculated as following

$$CH_4\ \text{selectivity}(\%) = \frac{CH_{4\,out}}{CO_{2\,in} - CO_{2\,out}} \times 100\%$$

$$CO\ \text{selectivity}(\%) = \frac{CO_{\,out}}{CO_{2\,in} - CO_{2\,out}} \times 100\%$$

where $CO_{2\,in}$ and $CO_{2\,out}$ represent the CO_2 concentration in the inlet and outlet respectively, and $CH_{4\,out}$ and $CO_{\,out}$ represent the amount of formed CH_4 and CO, respectively.

3. Results and discussion

3.1. Basic characterization of the catalysts

Fig. 1 presented the XRD pattern of all the catalysts. The diffraction peaks observed at 2θ = 21.9°, 28.2°, 31.1° and 35.8° are assigned to diffraction planes (111), (021), (112) and (220) of $AlPO_4$-tridymite crystal structure (JCPDS No. 11-0500) with no impurity phases [56]. The small peak at 20.6° may be due to the presence of structural defects [57]. The peak intensity increased with phosphorous content, suggesting the growth of $AlPO_4$-tridymite crystal phase. All the phosphorus loaded samples exhibited no characteristic diffraction peaks related with α-Al_2O_3 and NiO phases. 5 wt% NiO-Al_2O_3 catalyst exhibited main peaks at 2θ of 19.8°, 32.7°, 37.3°, 39.5°, 45.6°, 60.6°, 66.9° are assigned to diffraction planes (111), (220), (311), (222), (400), (511) and (440) of cubic γ-Al_2O_3 crystal phase (JCPDS No. 29-0063) [58]. There is no obvious signal of NiO phase detected in the XRD patterns of 5 wt% NiO-Al_2O_3 catalyst except a low intense peak at 2θ = 43.4° as a result of overlapping with the γ-Al_2O_3 peaks and low NiO content.

The BET surface area, pore volume and pore size of the catalysts were summarized in Table 1. All the catalysts showed type H3 hysteresis loop indicating the presence of slit shaped pores. The pore size distribution reveals the existence of mesopores in the range 2–9 nm. It is clear that the introduction of phosphorus into the 5 wt% NiO-Al_2O_3 results in considerable decrease in the surface area and pore volume with 22.67 m^2/g and 0.06 cm^3/g respectively for 5 wt% NiO-20P-Al_2O_3 in comparison with 100.52 m^2/g and 0.26 cm^3/g for 5 wt% NiO-Al_2O_3. This can be attributed to the blocking of pores of 5 wt% NiO-Al_2O_3 after phosphorus loading.

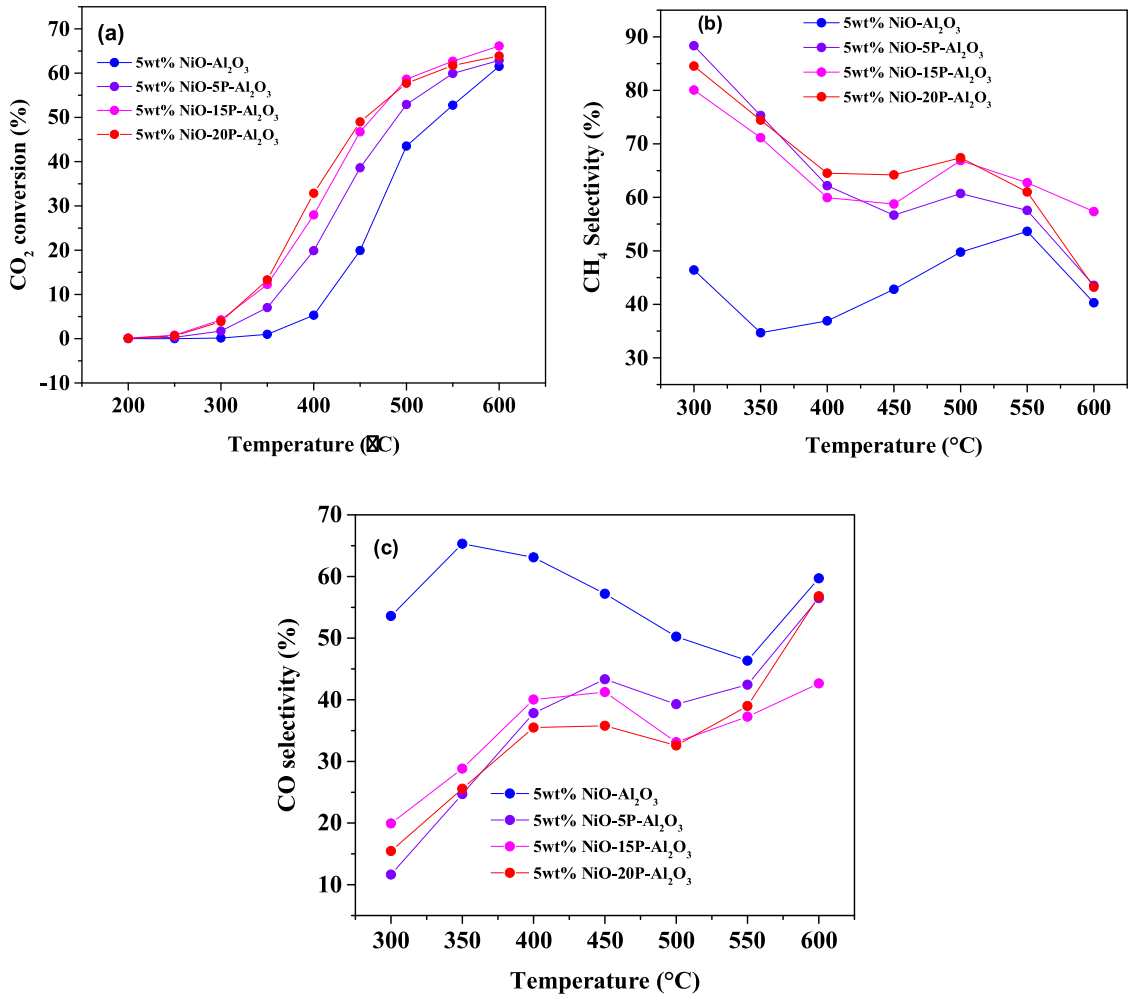

Fig. 4. CO_2 conversion on 5 wt% NiO-xP-Al_2O_3 (x = 0, 5, 15, 20) catalysts (a), CH_4 selectivity for CO_2 hydrogenation on 5 wt% NiO-xP-Al_2O_3 (x = 0, 5, 15, 20) catalysts (b) and CO selectivity for CO_2 hydrogenation on 5 wt% NiO-xP-Al_2O_3 (x = 0, 5, 15, 20) catalysts (c).

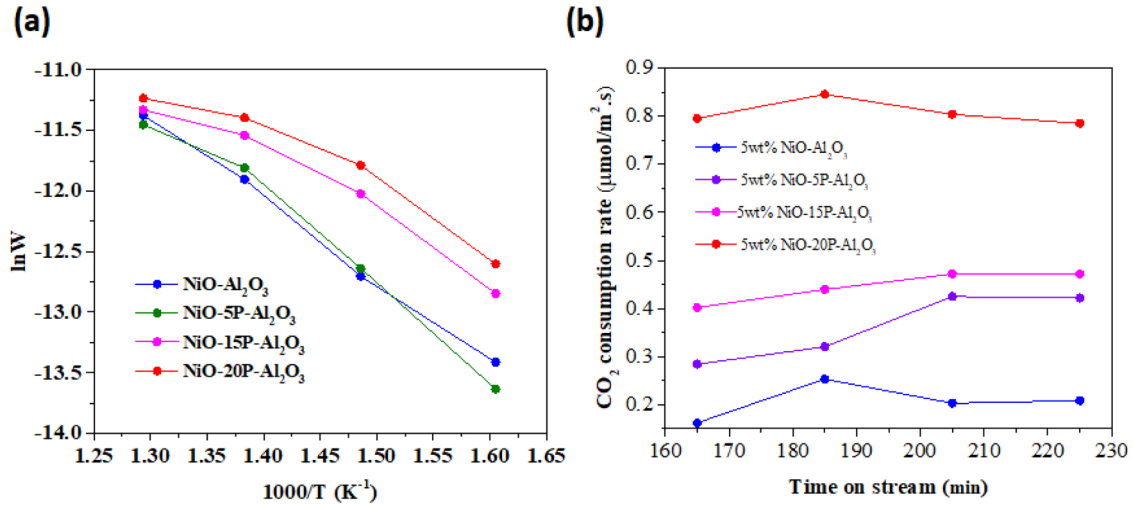

Fig. 5. Arrhenius plot for 5 wt% NiO-xP-Al_2O_3 (x = 0, 5, 15, 20) catalysts (a); Time on stream study over 5 wt% NiO-xP-Al_2O_3 (x = 0, 5, 15, 20) catalysts at 600 °C (b).

The morphology and particle size of some of the catalytically active catalysts were examined by TEM measurements and shown in Fig. 2. All the catalysts show nanoobjectives with porous structures with a building blocks of spherical shaped morphology with the size of ~2−15 nm.

The reducibility of the catalysts was studied by the H_2-TPR technique and the results are shown in Fig. 3. 5 wt% NiO-Al_2O_3 catalyst exhibited two reduction peaks. The low temperature peak at 406 °C was attributed to reduction of NiO not bound with Al_2O_3 and high temperature peak at 594 °C to the reduction of NiO that weakly interacted

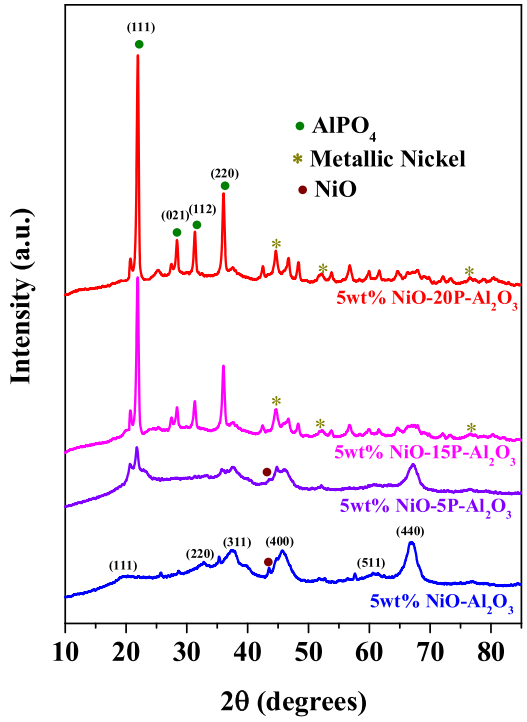

Fig. 6. XRD pattern of used 5 wt% NiO-xP-Al_2O_3 (x = 0, 5, 15, 20) catalysts.

with Al_2O_3 [59–62].

When phosphorus was added into the NiO-Al_2O_3 catalyst, there is a shift in reduction peaks of NiO towards lower temperature indicates that the addition of phosphorus facilitates the reduction of NiO. This observation corroborated well according to the previous work reported over Pd/xP-OMA catalyst [63]. The total H_2 consumptions have been summarized in Table 2.

3.2. Catalytic performance of the Phosphorous-loaded NiO/Al_2O_3 catalysts in CO_2 hydrogenation reaction

The catalytic performances of all the 5 wt% NiO-xP-Al_2O_3 (x = 0, 5, 15, 20) catalysts were evaluated at atmospheric pressure in the temperature range from 200 °C to 600 °C. The CO_2 conversion is shown in Fig. 4a. CO_2 conversion increased with temperature raising from 200 − 600 °C. All the catalysts reach the highest conversion at 600 °C with 61.54 %, 62.89 %, 63.88 % and 66.13 % respectively for 5 wt% NiO-Al_2O_3, 5 wt% NiO-5P-Al_2O_3, 5 wt% NiO-15P-Al_2O_3 and 5 wt% NiO-20P-Al_2O_3. The CO_2 conversion decreases in the order 5 wt% NiO-20P-Al_2O_3 > 5 wt% NiO-15P-Al_2O_3 > 5 wt% NiO-5P-Al_2O_3 > 5 wt% NiO-Al_2O_3.

The main products identified during the catalytic reaction were CO and CH_4. The CH_4 and CO selectivity results are shown in Fig. 4b and c respectively. CH_4 selectivity also depends on phosphorus loading, with 5 wt% NiO-xP-Al_2O_3 (x = 5, 15, 20) catalysts forming high CH_4 than 5 wt% NiO-Al_2O_3 catalyst. The CH_4 selectivity is high at low temperature and decreases to 64.2 %, 58.8 % and 56.7 % for 5 wt% NiO-20P-Al_2O_3, 5 wt% NiO-15P-Al_2O_3 and 5 wt% NiO-5P-Al_2O_3 catalysts respectively at 450 °C and then increased and decreased. The CO selectivity first increases then decreases and then again increases as the temperature increases. 5 wt% NiO-Al_2O_3 catalyst displayed higher CO selectivity. Gao et al. reported that, above 450 °C the formation of CO increases as a result of reverse water gas shift reaction while the CH_4 formation decreases as a result of exothermic nature of CO_2 methanation [64].

Fig. 5a shows the Arrhenius plot for CO_2 hydrogenation over all the 5 wt% NiO-xP-Al_2O_3 (x = 0, 5, 15, 20) catalysts. The apparent activation energies were calculated from the slopes in the temperature

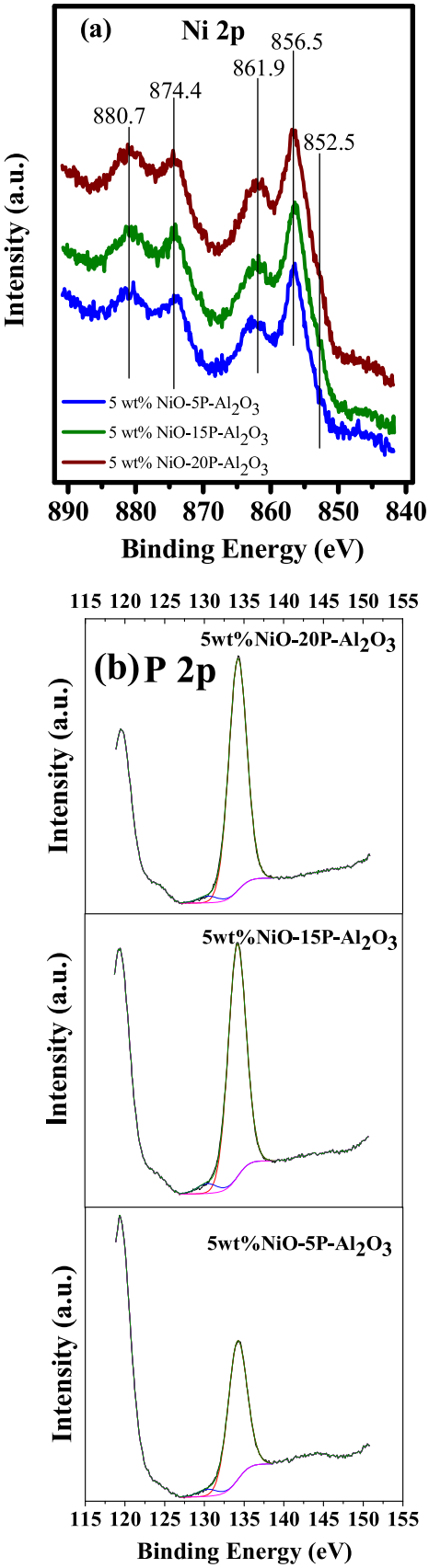

Fig. 7. XPS (a) Ni 2p (b) P 2p spectra of 5 wt% NiO-xP-Al_2O_3 (x = 5, 15, 20) catalysts.

Table 3
Binding Energy (eV) and Atomic Percentages (%) of Ni, Al, P, C and O elements as well as the phosphate and phosphide ratio obtained from XPS spectra of 5 wt% NiO-xP-Al_2O_3 (x = 0, 5, 15, 20) catalysts.

Catalysts	Ni 2p		Al 2p		P 2p		C 1 s		O 1 s		P 2p			
	B.E (eV)	%	B.E (eV)	%	B.E (eV)	%	B.E (eV)	%	B.E (eV)	%	Phosphate		Phosphide	
											B.E (eV)	Ratio %	B.E (eV)	Ratio %
5 wt% NiO-5P-Al_2O_3	852.5 856.5 861.9 874.4 880.7	0.78	74.2	23.58	134.15 130.37	7.75	284.78 286.48 288.84	10.73	531.90 530.63	57.16	134.15	95.08	130.37	4.92
5 wt% NiO-15P-Al_2O_3	852.5 856.5 861.9 874.4 880.7	1.15	74.1	20.11	134.17 130.39	11.58	284.80 286.38 288.77	9.61	532.17 530.27	57.55	134.17	95.4	130.39	4.6
5 wt% NiO-20P-Al_2O_3	852.5 856.5 861.9 874.4 880.7	1.27	74.4	18.05	134.21 130.43	13.61	284.80 286.47 288.69	10.65	532.28 530.13	56.4	134.21	96.87	130.43	3.13

range of 350−450 °C resulting in values of 56.3 kJ mol^{-1} for 5 wt% NiO-Al_2O_3, 68.3 kJ mol^{-1} for 5 wt% NiO-5P-Al_2O_3, 49.1 kJ mol^{-1} for 5 wt%NiO-15P-Al_2O_3 and 45.5 kJ mol^{-1} for 5 wt% NiO-20P-Al_2O_3. The apparent activation energy decreases with increase in phosphorus loading. 5 wt% NiO-20P-Al_2O_3 catalyst had the lowest apparent activation energy and this is in line with the catalytic activity.

Fig. 5b shows the time on stream results of all the catalysts for CO_2 hydrogenation at 600 °C. It can be seen that all the catalysts exhibit almost similar stability indicates that phosphorus addition does not improve the stability of the catalysts.

3.3. Characterization of the used catalysts

The used catalysts have been characterized by XRD in order to identify possible structural changes (Fig. 6). Besides NiO and $AlPO_4$ form, the XRD patterns revealed new peaks at 2θ = 44.5°, 51.8° and 76.3° for metallic nickel (JCPDS No. 65-2865) [65]. This metallic nickel is supposed to be formed during the pre-treatment with H_2 prior to the catalytic reaction and is responsible for H_2 dissociation during CO_2 hydrogenation.

For better understanding of the outstanding activity of phosphorous loaded catalysts, XPS studies were performed on the spent catalysts. The XPS was measured to study the chemical composition and valence states of the surface of the used 5 wt% NiO-xP-Al_2O_3 (x = 5, 15, 20) catalysts. The core level Ni 2p spectrum is shown in Fig. 7a. The peak at binding energy of 856.5 eV is ascribed to Ni $2p_{3/2}$ and another peak at binding energy of 874.4 eV is ascribed to Ni $2p_{1/2}$. The two relatively weak peaks at 861.9 eV and 880.7 eV belong to shakeup satellites indicating the presence of NiO [66]. The small shoulder peak at 852.7 eV is ascribed to the presence of metallic nickel [67]. The peak at 74.4 eV is ascribed to the presence of either Al_2O_3 or $AlPO_4$ [68]. However, based on the XRD results of the used catalyst, it could be expected as $AlPO_4$. Fig. 7b. shows P 2p XPS spectra. The peak at 134.4 eV is ascribed to the presence of $AlPO_4$ [69]. The small peak at 130.3 eV can be assigned to the Ni_2P/Ni_5P_{12} arising from the interaction of nickel with phosphorus [70]. This indicates the existence of Ni/NiO/Ni_2P/Ni_5P_{12}/$AlPO_4$ interfacial species in the catalyst during the reaction and this interfacial species increased with phosphorus loading and can be correlated with the higher catalytic activity.

The formation ratio of the metal-phosphide is relatively low ~3−5 % (Table 3) and this atomic concentration is decreasing with the rising of the phosphate content. However, the nickel enrichment in the surface layer presumable in Ni_2P/Ni_5P_{12} form is very likely according to the P 2p spectra. The authors assume that could be responsible for the enhanced catalytic activity. In the C 1s XPS spectra, three peaks were identified. The first peak at 284.78 eV is assigned to the CC and CH−− hydrocarbon and the second peak at 286.48 eV is assigned to CO−H arising from surface contamination. The third peak at 288.84 eV are assigned to CO and OCO=−= species, which can be attributed to a surface contamination component or a solvent degradation product. In the O 1s XPS spectra, two peaks were identified. The first peak at 531.9 eV is assigned to CO= and the second peak at 530.63 eV is assigned to the lattice oxygen, O−CO =[71]. The corresponding binding energies and atomic percentages as well as the phosphate and phosphide ratio according to the deconvoluted XPS spectra are reported in Table 3.

4. Conclusion

5 wt% NiO-xP-Al_2O_3 catalysts were prepared by a modified sol-gel method. The effect of phosphorus addition on NiO-Al_2O_3 catalyst in CO_2 hydrogenation was investigated. The BET surface area decreased with increasing phosphorus doping. The phosphorus loaded NiO-Al_2O_3 exhibited enhanced performance towards CO_2 hydrogenation compared with pure NiO-Al_2O_3. Ni/NiO/Ni_2P/Ni_5P_{12}/$AlPO_4$ interfacial species were detected as active species on the used catalysts by X-ray photoelectron spectroscopy. The formation ratio of the metal-phosphide is relatively low ~3−5 %, and this atomic concentration is decreasing with the rising of the phosphate content. However, the nickel enrichment in the surface layer presumable in Ni_2P/Ni_5P_{12} form is very likely according to the P 2p spectra and the authors assume that could be responsible for the enhanced catalytic activity. This work will not only help in understanding the role phosphorus in CO_2 hydrogenation reaction but also provide insights for future design and development of high performance phosphorus loaded catalysts.

Credit author statement

The authors have nothing to declare about Credit of Statement.

Declaration of Competing Interest

The authors declare no competing financial interest.

Acknowledgements

This paper was supported by the Hungarian Research Development and Innovation Office through grants NKFIH OTKA PD 120877 of AS. ÁK, and KZ is grateful for the fund of NKFIH (OTKA)K112531 & NN110676 and K120115, respectively. The financial support of the Hungarian National Research, Development and Innovation Office through the GINOP-2.3.2-15-2016-00013 project "Intelligent materials based on functional surfaces - from syntheses to applications" and the Ministry of Human Capacities through the EFOP-3.6.1-16-2016-00014 project and the 20391-3/2018/FEKUSTRAT are acknowledged.

References

[1] W. Zhou, K. Cheng, J. Kang, C. Zhou, V. Subramanian, Q. Zhang, Y. Wang, Chem. Soc. Rev. (2019).
[2] M. Aresta, A. Dibenedetto, A. Angelini, Chem. Rev. 114 (2013) 1709–1742.
[3] A. Sápi, G. Halasi, J. Kiss, D.G. Dobó, K.N.L. Juhász, V.J. Kolcsár, Z. Ferencz, G. Vári, V. Matolin, A.S. Erdőhelyi, J. Phys. Chem. C 122 (2018) 5553–5565.
[4] A. Sápi, T. Rajkumar, M. Ábel, A. Efremova, A. Grósz, A. Gyuris, K.B. Ábrahámné,

I. Szenti, J. Kiss, T. Varga, J. Co2 Util. 32 (2019) 106–118.
[5] T. Rajkumar, A. Sápi, M. Ábel, F. Farkas, J.F. Gómez-Pérez, Á. Kukovecz, Z. Kónya, Catal. Letters (2019) 1–10.
[6] J.A. Turner, Science 305 (2004) 972–974.
[7] S. Kattel, P. Liu, J.G. Chen, J. Am. Chem. Soc. 139 (2017) 9739–9754.
[8] H. Yang, C. Zhang, P. Gao, H. Wang, X. Li, L. Zhong, W. Wei, Y. Sun, Catal. Sci. Technol. 7 (2017) 4580–4598.
[9] M.D. Porosoff, B. Yan, J.G. Chen, Energy Environ. Sci. 9 (2016) 62–73.
[10] Y. Xu, J. Liu, J. Wang, G. Ma, J. Lin, Y. Yang, Y. Li, C. Zhang, M. Ding, ACS Catal. 9 (2019) 5147–5156.
[11] J. Su, H. Zhou, S. Liu, C. Wang, W. Jiao, Y. Wang, C. Liu, Y. Ye, L. Zhang, Y. Zhao, Nat. Commun. 10 (2019) 1297.
[12] J.H. Kwak, L. Kovarik, J.N. Szanyi, ACS Catal. 3 (2013) 2094–2100.
[13] A. Goguet, F. Meunier, J. Breen, R. Burch, M. Petch, A.F. Ghenciu, J. Catal. 226 (2004) 382–392.
[14] X. Zhu, X. Qu, X. Li, J. Liu, J. Liu, B. Zhu, C. Shi, Chin. J. Catal. 37 (2016) 2053–2058.
[15] S.V. Lambeets, C.D. Barroo, S. Owczarek, L. Jacobs, E. Genty, N. Gilis, N. Kruse, T. Visart De Bocarmé, J. Phys. Chem. C 121 (2017) 16238–16249.
[16] A. Aitbekova, L. Wu, C.J. Wrasman, A. Boubnov, A.S. Hoffman, E.D. Goodman, S.R. Bare, M. Cargnello, J. Am. Chem. Soc. 140 (2018) 13736–13745.
[17] C. Zhao, X. Dai, T. Yao, W. Chen, X. Wang, J. Wang, J. Yang, S. Wei, Y. Wu, Y. Li, J. Am. Chem. Soc. 139 (2017) 8078–8081.
[18] D. Williamson, C. Herdes, L. Torrente-Murciano, M.D. Jones, D. Mattia, ACS Sustain. Chem. Eng. (2019).
[19] R. Mutschler, E. Moioli, W. Luo, N. Gallandat, A. Züttel, J. Catal. 366 (2018) 139–149.
[20] J. Martins, N. Batail, S. Silva, S. Rafik-Clément, A. Karelovic, D.P. Debecker, A. Chaumonnot, D. Uzio, Catal. Commun. 58 (2015) 11–15.
[21] L. Falbo, C.G. Visconti, L. Lietti, J. Szanyi, Appl. Catal. B (2019) 117791.
[22] Y. Wang, H. Arandiyan, J. Scott, K.-F. Aguey-Zinsou, R. Amal, Acs Appl. Energy Mater. 1 (2018) 6781–6789.
[23] J. Li, Y. Lin, X. Pan, D. Miao, D. Ding, Y. Cui, J. Dong, X. Bao, ACS Catal. (2019).
[24] W. Li, Y. Liu, M. Mu, F. Ding, Z. Liu, X. Guo, C. Song, Appl. Catal. B 254 (2019) 531–540.
[25] D. Beierlein, D. Häussermann, M. Pfeifer, T. Schwarz, K. Stöwe, Y. Traa, E. Klemm, Appl. Catal. B 247 (2019) 200–219.
[26] S. Li, S. Guo, D. Gong, N. Kang, K.-G. Fang, Y. Liu, Int. J. Hydrogen Energy 44 (2019) 1597–1609.
[27] A. Kim, C. Sanchez, B. Haye, C. Boissière, C. Sassoye, D.P. Debecker, Acs Appl. Nano Mater. (2019).
[28] S. Lee, Y.H. Lee, D.H. Moon, J.Y. Ahn, D.D. Nguyen, S.W. Chang, S. Kim, Ind. Eng. Chem. Res. (2019).
[29] X. Jia, X. Zhang, N. Rui, X. Hu, C.-j. Liu, Appl. Catal. B 244 (2019) 159–169.
[30] X. Zhang, S.D. House, Y. Tang, L. Nguyen, Y. Li, A.A. Opalade, J.C. Yang, Z. Sun, F.F. Tao, ACS Sustain. Chem. Eng. 6 (2018) 6467–6477.
[31] Z.-F. Jiao, J.-X. Zhao, X.-N. Guo, X.-L. Tong, B. Zhang, G.-Q. Jin, Y. Qin, X.-Y. Guo, Catal. Sci. Technol. 9 (2019) 2266–2272.
[32] H. Liu, Y. He, K. Nagashima, G. Meng, T. Dai, B. Tong, Z. Deng, S. Wang, N. Zhu, T. Yanagida, Sens. Actuators B Chem. 293 (2019) 342–349.
[33] M. Yin, Z. Zhu, J. Alloys. Compd. 789 (2019) 941–947.
[34] Z. Zhu, L. Zheng, S. Zheng, J. Chen, X. Xing, D. Feng, D. Yang, J. Mater. Chem. A 7 (2019) 10456–10463.
[35] Y. Teng, H. Zhao, Z. Zhang, Y. Li, H. Liu, Mater. Lett. 246 (2019) 141–143.
[36] Y. Hong, J. Yang, J. Xu, W.M. Choi, Curr. Appl. Phys. 19 (2019) 715–720.
[37] F. Ding, A. Zhang, M. Liu, Y. Zuo, K. Li, X. Guo, C. Song, Ind. Eng. Chem. Res. 53 (2014) 17563–17569.
[38] J. Liu, A. Zhang, X. Jiang, M. Liu, J. Zhu, C. Song, X. Guo, Ind. Eng. Chem. Res. 57 (2018) 9120–9126.
[39] J. Sun, Y. Wang, H. Zou, X. Guo, Z.-j. Wang, J. Energy Chem. 29 (2019) 3–7.
[40] W. Cai, Y. Hu, J. Chen, G. Zhang, T. Xia, CrystEngComm 14 (2012) 972–977.
[41] M. Trueba, S.P. Trasatti, Eur. J. Inorg. Chem. 2005 (2005) 3393–3403.
[42] S. Das, A. Bag, R.K. Gupta, M. Sengupta, A. Bordoloi, Acs Appl. Energy Mater. 1 (2018) 4414–4419.
[43] Y. Zhan, Y. Wang, D. Gu, C. Chen, L. Jiang, K. Takehira, Appl. Surf. Sci. 459 (2018) 74–79.
[44] S.M. Sajjadi, M. Haghighi, Int. J. Energy Res. 43 (2019) 853–873.
[45] G. Zhu, K. Wu, L. Tan, W. Wang, Y. Huang, D. Liu, Y. Yang, ACS Sustain. Chem. Eng. 6 (2018) 10078–10086.
[46] Q. Li, Z. Yi, Y. Cheng, X. Wang, D. Yin, L. Wang, Appl. Surf. Sci. 427 (2018) 354–362.
[47] Y. Feng, H. Zhang, L. Fang, W. Li, Y. Wang, J. Mater. Chem. A 4 (2016) 11507–11515.
[48] X. Li, Z. Mu, J. Hu, Z. Cui, Sens. Actuators B Chem. 232 (2016) 143–149.
[49] Y. Liu, F. Liu, J. Bai, T. Liu, Z. Yu, M. Dai, L. Zhou, H. Wang, Y. Zhang, H. Suo, Sens. Actuators B Chem. (2019).
[50] J. Rong, T. Zhang, F. Qiu, M. Chen, Korean J. Chem. Eng. 34 (2017) 41–53.
[51] C. Lei, X. Zhu, Y. Le, B. Zhu, J. Yu, W. Ho, RSC Adv. 6 (2016) 10272–10279.
[52] W. Gu, M. Shen, X. Chang, Y. Wang, J. Wang, J. Alloys. Compd. 441 (2007) 311–316.
[53] J. Wang, Y. Wang, J. Wen, M. Shen, W. Wang, Microporous Mesoporous Mater. 121 (2009) 208–218.
[54] M. Shen, L. Song, J. Wang, X. Wang, Catal. Commun. 22 (2012) 28–33.
[55] X. Chen, X. Zheng, W. Lin, D. Chen, Y. Zheng, L. Jiang, Powder Technol. 338 (2018) 869–877.
[56] Y.-f. Liu, Z.-p. Yang, Q.-m. Yu, J. Alloys. Compd. 509 (2011) L199–L202.
[57] J. Campelo, M. Jaraba, D. Luna, R. Luque, J. Marinas, A. Romero, J. Navio, M. Macias, Chem. Mater. 15 (2003) 3352–3364.
[58] M. Shah, A. Bordoloi, A.K. Nayak, P. Mondal, Fuel Process. Technol. 192 (2019) 21–35.
[59] S. Mahammadunnisa, P. Manoj Kumar Reddy, B. Ramaraju, C. Subrahmanyam, Energy Fuels 27 (2013) 4441–4447.
[60] T. Borowiecki, W. Gac, A. Denis, Appl. Catal. A Gen. 270 (2004) 27–36.
[61] J. Zhang, H. Xu, X. Jin, Q. Ge, W. Li, Appl. Catal. A Gen. 290 (2005) 87–96.
[62] S. Abate, C. Mebrahtu, E. Giglio, F. Deorsola, S. Bensaid, S. Perathoner, R. Pirone, G. Centi, Ind. Eng. Chem. Res. 55 (2016) 4451–4460.
[63] X. Chen, Y. Zheng, F. Huang, Y. Xiao, G. Cai, Y. Zhang, Y. Zheng, L. Jiang, ACS Catal. 8 (2018) 11016–11028.
[64] J. Gao, Y. Wang, Y. Ping, D. Hu, G. Xu, F. Gu, F. Su, RSC Adv. 2 (2012) 2358–2368.
[65] X. Fang, J. Zhang, J. Liu, C. Wang, Q. Huang, X. Xu, H. Peng, W. Liu, X. Wang, W. Zhou, J. Co2 Util. 25 (2018) 242–253.
[66] Y. Fu, C. Zhu, H. Wang, Y. Dou, W. Shi, M. Shao, H. Huang, Y. Liu, Z. Kang, Inorg. Chem. Front. 5 (2018) 1646–1652.
[67] L. Sciortino, F. Giannici, A. Martorana, A.M. Ruggirello, V.T. Liveri, G. Portale, M.P. Casaletto, A. Longo, J. Phys. Chem. C 115 (2011) 6360–6366.
[68] S. Verdier, L. El Ouatani, R. Dedryvere, F. Bonhomme, P. Biensan, D. Gonbeau, J. Electrochem. Soc. 154 (2007) A1088–A1099.
[69] J.A. Rotole, P.M. Sherwood, Surf. Sci. Spectra 5 (1998) 60–66.
[70] Y. Chen, H. She, X. Luo, G.-H. Yue, D.-L. Peng, J. Cryst. Growth 311 (2009) 1229–1233.
[71] R. Al-Gaashani, A. Najjar, Y. Zakaria, S. Mansour, M. Atieh, Ceram. Int. 45 (2019) 14439–14448.